Immunoresponsive Gene 1 and Itaconate Inhibit Succinate Dehydrogenase to Modulate Intracellular Succinate Levels*

Thekla Cordes[‡], Martina Wallace[‡], Alessandro Michelucci[§¶], Ajit S. Divakaruni[‖], Sean C. Sapcariu[¶], Carole Sousa[§¶], Haruhiko Koseki[**], Pedro Cabrales[‡], Anne N. Murphy[‖], Karsten Hiller[¶], and Christian M. Metallo[‡‡‡1]

From the Departments of [‡]Bioengineering and [‖]Pharmacology and [‡‡]Institute of Engineering in Medicine, University of California, San Diego, La Jolla, California 92093, the [§]NORLUX Neuro-Oncology Laboratory, Department of Oncology, Luxembourg Institute of Health, 1526 Luxembourg, Luxembourg, the [¶]Luxembourg Centre for Systems Biomedicine, University of Luxembourg, 4362 Esch-Belval, Luxembourg, and the [**]RIKEN Center for Integrative Medical Sciences, Yokohama, Kanagawa 230-0045, Japan

Metabolic reprogramming is emerging as a hallmark of the innate immune response, and the dynamic control of metabolites such as succinate serves to facilitate the execution of inflammatory responses in macrophages and other immune cells. Immunoresponsive gene 1 (*Irg1*) expression is induced by inflammatory stimuli, and its enzyme product *cis*-aconitate decarboxylase catalyzes the production of itaconate from the tricarboxylic acid cycle. Here we identify an immunometabolic regulatory pathway that links *Irg1* and itaconate production to the succinate accumulation that occurs in the context of innate immune responses. Itaconate levels and *Irg1* expression correlate strongly with succinate during LPS exposure in macrophages and non-immune cells. We demonstrate that itaconate acts as an endogenous succinate dehydrogenase inhibitor to cause succinate accumulation. Loss of itaconate production in activated macrophages from *Irg1*$^{-/-}$ mice decreases the accumulation of succinate in response to LPS exposure. This metabolic network links the innate immune response and tricarboxylic acid metabolism to function of the electron transport chain.

Immune cells must sense cues from the extracellular microenvironment and respond rapidly to protect against bacteria, viruses, or other pathogens (1). An emerging hallmark of inflammation and the innate immune system of cells is metabolic reprogramming (2). One of the most general metabolic changes that occurs under proinflammatory conditions is a biochemical switch from oxidative phosphorylation to aerobic glycolysis (3–5), which is mediated, in part, via stabilization of hypoxia-inducible factor 1α (HIF-1α)[2] after pathogen infection (6), LPS binding to toll-like receptors (7), or by cytokine exposure (8). Although it is known that macrophages undergo drastic metabolic reprogramming upon exposure to inflammatory stimuli, the underlying mechanisms driving this response are not completely understood.

Increased succinate levels in macrophages are important mediators of the inflammatory response, linking metabolism to innate immunity. In addition to its role in TCA metabolism, succinate acts as a regulatory signal enhancing *Il-1β* expression through stabilization of HIF-1α, which, in turn, influences the function of various other metabolic pathways (9). Succinate inhibits the hydroxylation of HIF-1α by *EGLN1*, resulting in pseudohypoxic HIF-1α stabilization under normoxic conditions (10–12). Various mechanisms have been proposed as the cause of succinate accumulation, including increased glutamine anaplerosis and oxidation in the TCA cycle or increased flux through the GABA shunt (9, 13), although glycolytic metabolism is a prerequisite (14). However, the specific driver(s) of this phenomenon has/have not yet been identified. Given the central role of succinate as a metabolic signal in inflammation, elucidation of the metabolic pathway(s) involved in succinate accumulation and its/their regulation may provide new avenues for controlling this process.

Metabolites are important functional triggers that can regulate the activity of enzymes via substrate/product inhibition, posttranslational modifications, or allosteric interactions (15). Beyond their direct roles as substrates and products, metabolites often serve as substrates for posttranslational modifications, as shown for succinate to succinylate proteins (9). On the other hand, fructose 1,6-bisphosphate (16), serine, and other amino acids can allosterically influence the activity of the enzyme pyruvate kinase isoform M2 (PKM2) (17, 18). Recently, synthesis of the antimicrobial metabolite itaconate was identified in mammalian immune cells as being selectively up-regulated under proinflammatory conditions (19). Itaconate exhibits an antibiotic function (20) via inhibition of isocitrate lyase, a key enzyme of the glyoxylate shunt needed by many bacteria to survive during infection (21–23). In mammals, itaconate is pro-

1 To whom correspondence should be addressed: Dept. of Bioengineering, University of California, San Diego, 9500 Gilman Dr., MC-0412 PFBH 204, La Jolla, CA 92093. Tel.: 858-534-8209; E-mail: cmetallo@ucsd.edu.

2 The abbreviations used are: HIF, hypoxia-inducible factor; TCA, tricarboxylic acid; CAD, *cis*-aconitate decarboxylase; SDH, succinate dehydrogenase; BMDM, bone marrow-derived macrophage; MSTFA, 2,2,2-trifluoro-*N*-methyl-*N*-trimethylsilyl-acetamide; MTBSTFA, *N*-tert-butyldimethylsilyl-*N*-methyltrifluoroacetamide; OCR, oxygen consumption rate.

duced through the decarboxylation of the TCA cycle intermediate *cis*-aconitate, which is catalyzed by mammalian *cis*-aconitate decarboxylase (CAD, also known as immune-responsive gene 1 (IRG1) protein) encoded by immunoresponsive gene 1 (*IRG1*) (20). Itaconate production represents one of two characteristic TCA cycle "break points" discovered in classically activated immune cells (24, 25). The first break occurs at isocitrate dehydrogenase, leading to the accumulation of citrate, the precursor for itaconate, and the second break occurs at succinate dehydrogenase (SDH), which may allow for succinate accumulation. Although itaconate has been shown previously to inhibit SDH *ex vivo* (26–28), and LPS-activated murine macrophages produced up to 8 mM intracellular itaconate (20), a potential role of endogenously produced itaconate in succinate accumulation under inflammatory conditions has not yet been addressed and is unknown.

To elucidate the role of itaconate in reprogramming immune cell metabolism, we modulated intracellular itaconate levels in primary bone marrow-derived macrophages (BMDMs), a macrophage cell line, as well as a lung adenocarcinoma cell line. In all cell models we observed metabolic changes reminiscent of SDH inhibition, including succinate accumulation. By measuring substrate-specific mitochondrial respiration, we demonstrated the inhibition of SDH by itaconate in a dose-dependent manner. Furthermore, stimulated BMDMs from *Irg1* KO mice failed to produce itaconate and exhibited decreased succinate accumulation compared with BMDMs from WT mice. Based on these studies, we have elucidated an *Irg1*-induced immunomodulatory pathway in macrophages whereby its product, itaconate, acts as an endogenously produced metabolic regulator of mitochondrial metabolism.

Experimental Procedures

Cell Culture and Isotopic Labeling—RAW 264.7 macrophages (29) (ATCC, TIB-71) and A549 cells (30) (ATCC, CCL-185) were maintained in high-glucose DMEM (Life Technologies) supplemented with 10% (v/v) FBS, 100 units·ml^{-1} penicillin/streptomycin, 25 mM glucose, and 4 mM L-glutamine. Cell lines tested negative for mycoplasma contamination using the MycoAlert mycoplasma detection kit (Lonza) according to the instructions of the manufacturer. Purified *Escherichia coli* LPS was used for the activation of RAW 264.7 macrophages and BMDMs at a concentration of 10 ng·ml^{-1}. A549 and RAW 264.7 cells and BMDMs were exposed to increasing itaconate concentrations (5, 10, and 25 mM) for 6 h. For isotopic labeling experiments, RAW 264.7 macrophages were cultured in DMEM (Sigma) supplemented with 25 mM glucose, 4 mM [1-^{13}C]glutamine (Cambridge Isotopes Inc.) and 10% (v/v) dialyzed FBS for 24 h prior to addition of LPS for 6 h. For isotope tracing with exposure to unlabeled itaconate, RAW 264.7 cells were exposed to labeled [U-^{13}C$_6$]glucose and [U-^{13}C$_5$]glutamine tracers over a period of three subcultures and then exposed further for 6 and 24 h to 10 mM unlabeled itaconate.

BMDMs—BMDM collection was approved by the Institutional Animal Care and Use Committee and was conducted according to the Guide for the Care and Use of Laboratory Animals (US National Research Council, 2010). BMDMs were isolated from femora and tibiae of C57BL/6J mice (The Jackson Laboratory, Bar Harbor, ME). Bones were collected in ice-cold PBS, cleaned of muscle, and flushed with 5 ml BMDM growth medium (DMEM, Life Technologies) supplemented with 10% (v/v) FBS, 100 units·ml^{-1} penicillin/streptomycin, 25 mM glucose, 4 mM L-glutamine, 20 ng·ml^{-1} recombinant-macrophage colony-stimulating factor (eBioscience), and 3.4 μl·l^{-1} β-mercaptoethanol). Cells were seeded at 5×10^6 cells on Petri dishes in 10 ml of growth medium. 5 ml of fresh growth medium was added on day 3. On day 6, BMDMs were collected and replated into 6-well tissue culture plates at a density of 5×10^5 cells/well in growth medium containing 2 ng·ml^{-1} recombinant-macrophage colony-stimulating factor. Metabolites were extracted on day 7.

For *Irg1* KO *versus* WT BMDM experiments, all animal procedures, such as handling and euthanasia, were performed according to the Federation of European Laboratory Animal Science Associations guidelines for the use of animals in research. The *Irg1* KO mice were generated by Dr. Haruhiko Koseki at the RIKEN Institute using stem cells purchased from the Knockout Mouse Project Repository under strain ID Irg1$^{tm1a(KOMP)Wtsi}$. Mice were anesthetized by intraperitoneal injection of 50 mg·kg^{-1} of ketamine hydrochloride and 5 mg·kg^{-1} xylazine hydrochloride, and bone marrow was isolated and cultured as described previously (31). Briefly, bone marrow was flushed from femora and tibiae of *Irg1* KO and age-matched C57BL/6 WT mice, and the resultant cell suspension was passed through a 70-μm filter (Greiner Bio-One). After 10 min of centrifuging at $250 \times g$, the supernatant was discarded, and the pellet was resuspended in 2 ml of hypotonic solution (170 mM NH$_4$Cl) for 5 min to allow lysis of any remaining extracellular red blood cells. Bone marrow-derived cells were plated in 12-well plates (Greiner Bio-One) at 5×10^5 cells/well. Cells were cultured for 6 days at 37 °C in RPMI 1640 VLE (Very Low Endotoxin) (Biochrom FG 1415) supplemented with 10% FBS and 20% conditioned medium from macrophage colony-stimulating factor-secreting L929 fibroblasts. After 6 days in culture, the BMDMs were used for experiments.

Metabolite Quantification—Metabolite levels of itaconate and TCA cycle intermediates were quantified using external standard curves (three biological replicates). For metabolite standard curves, increasing standard solutions were extracted under the conditions of sample preparation. Using the depicted standard curve, the metabolite quantity in each cell extract was calculated, taking into account cellular diameter (d, micrometers) of detached cells and cell number. We assumed a spherical shape and calculated the intracellular metabolite concentration using the following equation: [metabolite] = metabolite quantity (moles)/$(((4/3000) \pi (d/2)^3)$ cell number). Cell number and cell diameter were determined using a Countess automated cell counter (Invitrogen).

Cell Transfections—*Irg1* gain-of function experiments in A549 cells were performed as described previously (20). Briefly, A549 cells were transfected with the pCMV6-*Irg1* (OriGene) overexpressing plasmid or empty plasmid using Lipofectamine 2000 (Invitrogen) and further incubated for 24 h.

RNA Isolation and RT-PCR—Total RNA was purified from cultured cells using the Qiagen RNeasy mini kit (Qiagen)

according to the instructions of the manufacturer. First-strand cDNA was synthesized from total RNA using SuperScript III (Invitrogen) with 1 μl (50 μM)/reaction oligo(dT)20 as primer according to the instructions of the manufacturer. Individual 20-μl SYBR Green real-time PCR reactions consisted of 2 μl of diluted cDNA, 10 μl of fast SYBR Green Master Mix (Applied Biosystems), and 0.5 μl of each 10 μM forward and reverse primers. For standardization of quantification, L27 was amplified simultaneously. PCR was carried out in 96-well plates on an Applied Biosystems Viia^{TM} 7 real-time PCR system using the following program: 95 °C for 20 s, 40 cycles of 95 °C for 1 s, and 60 °C for 20 s (*Irg1*, GCAACATGATGCTCAAGTCTG (forward) and TGCTCCTCCGAATGATACCA (reverse); *L27*, ACATTGACGATGGCACCTC (forward) and GCTTGGCG-ATCTTCTTCTTG (reverse)).

Oxygen Consumption Measurements—Respiration was measured in adherent monolayers of RAW 264.7 macrophages or BMDMs using a Seahorse XF96 analyzer. RAW 264.7 macrophages were plated at 3×10^4 cells/well (for assays with permeabilized cells) and 4×10^4 cells/well (for assays with intact cells) and BMDMs at 5×10^4 cells/well 24 h before measurement. Intact cells were assayed in DMEM (Sigma, 5030) supplemented with 8 mM glucose, 3 mM glutamine, 3 mM pyruvate, and 2 mM HEPES. Cells were permeabilized with 3 nM perfringolysin O (commercially, XF PMP (XF Plasma Membrane Permeabilizer)) as described previously (32). Phosphorylating (state 3), succinate-driven respiration in permeabilized cells was measured in cells offered 4 mM ADP, 2 μM rotenone, two different succinate concentrations (2.5 and 10 mM), and increasing itaconate concentrations (0, 5, 10, and 25 mM). When measuring respiration on different respiratory substrates, permeabilized cells were offered succinate (10 mM)/rotenone (2 μM), glutamate/malate (each 10 mM), pyruvate/malate (each 10 mM), or ascorbate (10 mM) plus *N,N,N',N'*-tetramethyl-*p*-phenylenediamine (TMPD) (100 μM) and antimycin A (1 μM). Maximal respiration was calculated as the difference between protonophore-stimulated respiration (600 nM carbonyl cyanide *p*-trifluoromethoxyphenylhydrazone) and nonmitochondrial respiration (measured after addition of 1 μM antimycin A). All data are mean ± S.E. of two or three repeated experiments (with a minimum of five biological replicates per experiment) as indicated in the text. For assays with BMDMs, cells were obtained from three different mice.

GC-MS Sample Preparation and Analysis—Polar metabolites were extracted using methanol/water/chloroform as described previously (20). For medium metabolites, medium was centrifuged at 4 °C for 5 min at 300 × *g*. 10 μl of supernatant was added to 80 μl of a −20 °C 8:1 methanol/water mixture, mixed for 10 min at 4 °C, and centrifuged at 16,000 × *g* for 10 min at 4 °C. 80 μl was collected and evaporated under a vacuum at −4 °C. Metabolite derivatization was performed using a Gerstel MPS. Dried polar metabolites were dissolved in 15 μl of 2% (w/v) methoxyamine hydrochloride (Thermo Scientific) in pyridine and incubated for 60 min at 45 °C. An equal volume of 2,2,2-trifluoro-*N*-methyl-*N*-trimethylsilyl-acetamide (MSTFA) or *N*-*tert*-butyldimethylsilyl-*N*-methyltrifluoroacetamide (MTBSTFA) with 1% *tert*-butyl dimethylchlorosilane (Regis Technologies) was added and incubated further for

30 min at 45 °C. After derivatization, MSTFA-derivatized samples were analyzed as described previously (20). Briefly, derivatized samples were analyzed by GC-MS using a DB-35MS column (30 × 0.25 mm inner diameter × 0.25 μm, Agilent J&W Scientific) installed in an Agilent 7890A gas chromatograph interfaced with an Agilent 5975C mass spectrometer. For MTBSTFA-derivatized samples, the GC oven was held at 100 °C for 1 min, increased to 255 °C at 3.5 °C min^{-1}, increased to 320 °C at 15 °C min^{-1}, and held at 320 °C for 3 min. The total run time for one sample was 54.62 min. For *Irg1* KO *versus* WT BMDM metabolite measurements, the GC oven was held at 100 °C for 2 min, increased to 300 °C at 10 °C min^{-1}, and held at 325 °C for 3 min. The total run time for one sample was 26 min.

MSTFA-derivatized metabolites were determined using the following quantification ions: itaconate (*m/z* 259) and succinate (*m/z* 247). Metabolite levels and mass isotopomer distributions of MTBSTFA-derivatized samples were analyzed by integrating metabolite fragment ions (itaconate, *m/z* 301–310; succinate, *m/z* 289–294; citrate, *m/z* 459–469; α-ketoglutarate, *m/z* 346–355; malate, *m/z* 419–428; and fumarate, *m/z* 287–292) and corrected for natural abundance using in-house algorithms.

Statistical Analysis—All results shown as averages of one to three repeated experiments with each at least two biological replicates as indicated in the text. A repeated experiment is defined as a separate experiment temporally. Biological replicates are defined as separate spatial replicates (*i.e.* wells of a tissue culture plate) within an experiment. In the case of BMDMs, repeated experiments are defined as cells from different mice. Error bars indicate mean ± S.E. The statistical tool R (33) was used to calculate the Pearson correlation coefficient. For comparison of means between two different treatments, the statistical analysis was done by two-tailed Student's *t* test. *, $p < 0.05$; **, $p < 0.01$; ***, $p < 0.001$.

Results

Succinate and Itaconate Accumulate in LPS-activated RAW 264.7 Macrophages—To better understand the relationship between *Irg1*-mediated itaconate production and the reprogramming of TCA metabolism under LPS-stimulated conditions, we quantified the dynamics of itaconate and TCA intermediate abundances in RAW 264.7 macrophages over time. To elicit an immune response, we exposed RAW 264.7 macrophages to 10 ng·ml^{-1} LPS for 6 h, conditions that induce high expression of *Irg1* encoding CAD, the enzyme catalyzing itaconate production from *cis*-aconitate (20). Intriguingly, the levels of itaconate and succinate exhibited similar trends upon activation, in contrast to the dynamics of citrate, α-ketoglutarate, fumarate, and malate (Fig. 1*a*), suggesting that itaconate and succinate (or the enzymes metabolizing them) are regulated in a coordinated manner. Notably, basal oxygen consumption rates (OCR) remained unchanged compared with resting macrophages (Fig. 1*b*).

Exogenous Itaconate Drives Succinate Accumulation—To determine whether itaconate directly contributes to succinate accumulation, we next supplemented the growth medium of resting and LPS-activated murine RAW 264.7 macrophages
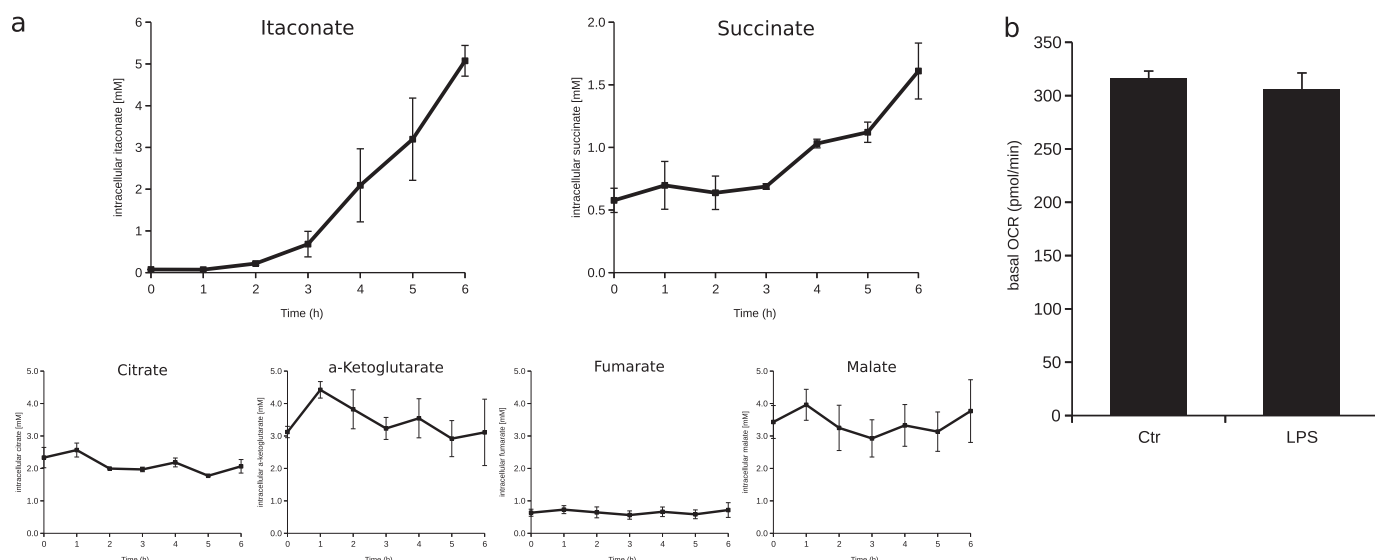
FIGURE 1. **Succinate and itaconate accumulate in LPS-activated murine RAW 264. 7 macrophages.** *a*, dynamics of itaconate, succinate, citrate, α-ketoglutarate, fumarate, and malate levels. Cells were exposed to 10 ng·ml^{-1} LPS, and metabolites were extracted every hour over a 6-h period. Graphs represent the mean ± S.E. of time-dependent, intracellular metabolite concentrations [mM] of two repeated experiments, each with three biological replicates. *b*, the basal OCR is unchanged in LPS-activated (*LPS*) macrophages compared with resting macrophages (*Ctr*). *Error bars* represent mean ± S.E. of two repeated experiments.

with increasing itaconate concentrations for 6 h and observed how intracellular itaconate levels correlated with those of various TCA cycle intermediates (Figs. 2, *a–f*). LPS-activated murine macrophages can produce up to 8 mM intracellular itaconate (20), but higher levels may accumulate in specific compartments (*e.g.* mitochondria). Therefore, we considered four different itaconate concentrations ranging from 0–25 mM. Exposure to exogenous itaconate resulted in increasing intracellular itaconate levels in a dose-dependent manner (Fig. 2*c*), indicating that cells have the capacity to take up itaconate from medium. However, medium itaconate levels were not appreciably affected (Fig. 2*g*). Interestingly, no mitochondrial or plasma membrane itaconate transporters have been described in mammalian cells to date.

We next calculated the Pearson correlation coefficient (*r*) between the intracellular abundance of itaconate and each TCA intermediate to gauge the relationship across each pair. Intriguingly, we observed that intracellular itaconate levels correlated strongly with succinate levels in resting (*r* = 0.99) as well as LPS-activated macrophages (*r* = 0.99) so that higher itaconate levels were associated with elevated succinate levels (Fig. 2*e*). Importantly, the levels of other TCA intermediates, including citrate, α-ketoglutarate, fumarate, and malate correlated poorly (or in some cases negatively) with intracellular itaconate levels (Fig. 2, *a*, *b*, *d*, and *f*). Because succinate accumulates after exposure to exogenous itaconate in RAW 264.7 macrophages (Fig. 2*e*) as well as BMDMs (Fig. 2*h*), these data suggest that LPS-induced itaconate production by mammalian CAD contributes to the elevated succinate levels observed in activated macrophages. Importantly, exposure to exogenous itaconate induces succinate accumulation in resting RAW 264.7 macrophages (Fig. 2*e*) as well as resting BMDMs (Fig. 2*h*), indicating that the mechanism through which itaconate acts is independent of other inflammatory signaling events.

Itaconate and Irg1-induced Succinate Accumulation Is Not Specific to Immune Cells—To further investigate whether itaconate reprograms TCA metabolism independent of inflammatory signals, we supplemented increasing itaconate concentrations (0, 5, 10, and 25 mM) to the growth medium of human A549 lung adenocarcinoma cells and quantified intracellular metabolite concentrations after 6 h. As before (Fig. 2*c*), uptake of extracellular itaconate from the medium was evidenced by increasing intracellular itaconate levels (Fig. 3*a*), whereas medium itaconate abundances did not change (Fig. 3*b*). Succinate levels increased linearly with itaconate levels and correlated strongly (*r* = 0.99), whereas other TCA cycle intermediates, including citrate, α-ketoglutarate, fumarate, and malate, did not accumulate (Fig. 3*a*). These results are consistent with our observations using RAW 264.7 macrophages (Fig. 2), and because A549 cells do not express *IRG1* (20) they suggest that itaconate-mediated succinate accumulation occurs even in the absence of an active inflammatory signaling cascade.

To determine whether CAD-mediated itaconate production can affect succinate levels in non-immune cells, we overexpressed *Irg1* in human A549 cells using a pCMV6-plasmid encoding murine *Irg1*. Itaconate was only produced at detectable levels in pCMV6 *Irg1*-overexpressing A549 cells (pm*Irg1*) compared with vector (pCMV6) controls (Fig. 3*c*). Notably, pm*Irg1* cells accumulated significantly higher amounts of succinate compared with pCMV6 controls (Fig. 3*d*), indicating that ectopic expression of CAD alone is sufficient to impact succinate levels. Collectively, these observations provide strong evidence that itaconate functions as metabolic trigger to modulate succinate levels.

Itaconate Is Not Metabolized to Succinate—One explanation for the above results could be that accumulated itaconate is metabolized to succinate directly or indirectly in macrophages. Indeed, *Pseudomonas* sp. can metabolize itaconate as a carbon
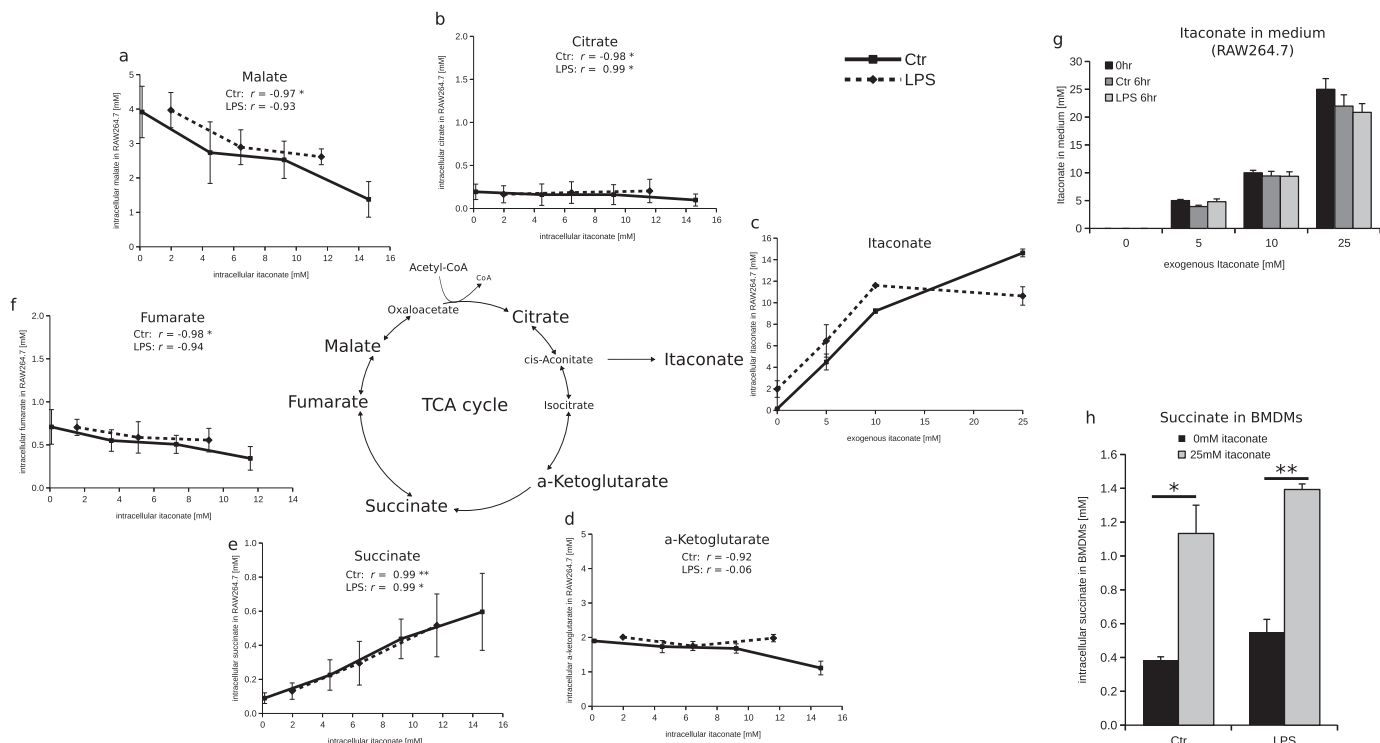
FIGURE 2. **Exogenous itaconate drives succinate accumulation.** Intracellular TCA cycle intermediate and itaconate quantification in resting (*Ctr*, *continuous line*) and LPS-activated (*LPS*, *dashed line*) RAW 264.7 macrophages after 6-h exposure to increasing extracellular itaconate concentrations (0, 5, 10, and 25 mM) (*a*, malate; *b*, citrate; *c*, itaconate; *d*, α-ketoglutarate; *e*, succinate; *f*, fumarate). Cells were exposed to 10 ng·ml^{-1} LPS for 6 h. Graphs represent the mean ± S.E. of intracellular metabolite concentrations [mM] of two repeated experiments, each with three biological replicates. Pearson correlation coefficient (*r*) represents correlation between intracellular itaconate and TCA cycle intermediate concentrations. *g*, medium itaconate levels of resting and LPS-activated RAW 264.7 macrophages (10 ng·ml^{-1} LPS) at 0 h (*black*) and after 6 h (*gray*). Data represent the mean ± S.E. of metabolite levels [mM] of three biological replicates. *h*, intracellular succinate quantification in resting and LPS-activated BMDMs after 6-h exposure to 0 mM (*black*) or 25 mM (*gray*) extracellular itaconate. Cells were exposed to 10 ng·ml^{-1} LPS for 6 h. Graphs represent the mean ± S.E. of succinate concentration [mM] obtained from two different mice, each with three biological replicates. *, $p < 0.05$; **, $p < 0.01$.

source through cleavage into pyruvate and acetyl-CoA (34), and a similar itaconate degradation pathway has been observed in isolated liver mitochondria (35). To exclude the possibility that degradation of itaconate to succinate occurs, we applied a [1-^{13}C]glutamine tracer to LPS-activated RAW 264.7 macrophages. During oxidative glutamine metabolism, decarboxylation of M1 α-ketoglutarate derived from this tracer results in M0 succinate. In contrast to the oxidative pathway, M1 α-ketoglutarate is converted to M1 isocitrate and citrate via reductive carboxylation (36), subsequently leading to M1 itaconate labeling. Thus, if itaconate is appreciably metabolized to succinate through the aforementioned degradation pathways, then we would detect significant labeling on succinate from this tracer (Fig. 4*a*). Although we observed high fractions of M1 itaconate isotopologues (~65%) because of itaconate production via reductive glutamine metabolism, no labeling was detected on succinate (Fig. 4*b*).

To further demonstrate that itaconate is not metabolized to succinate, we cultured ^{13}C-labeled resting and LPS-activated RAW 264.7 macrophages in the presence of 10 mM unlabeled itaconate and quantified succinate labeling. We exposed cells to labeled [U-^{13}C$_6$]glucose and [U-^{13}C$_5$] glutamine tracers over a period of three subcultures to obtain adequate isotope enrichment in succinate pools (Fig. 4*c*). Because labeling of succinate after exposure to exogenous, unlabeled itaconate was unchanged (even in the physi-

ological concentration used here) (Fig. 4*d*), these data therefore confirm that itaconate is not metabolized to succinate in these mammalian cells.

Itaconate Inhibits SDH—Although enhanced flux through succinate-producing pathways from glutamine or glucose is likely contributing to its accumulation in inflammatory cells, our results suggest that itaconate degradation does not occur. An alternative mechanism through which endogenous itaconate could influence succinate levels is through inhibition of SDH/complex II. Indeed, *in vitro* enzyme activity assays using isolated SDH and respiratory studies have indicated that itaconate can reduce the activity of SDH (27, 28, 37). Mammalian CAD is localized to mitochondria in murine macrophages (38); therefore, itaconate production within or near this compartment could modulate SDH activity and, subsequently, succinate levels. To investigate the potential for itaconate to act as an SDH inhibitor, we measured mitochondrial respiration in permeabilized murine RAW 264.7 macrophages and BMDMs. First, we exposed permeabilized macrophages to increasing itaconate concentrations (0–25 mM) in the presence of two different succinate concentrations (2.5 and 10 mM) with 2 μM rotenone. Succinate is the substrate for complex II (SDH) of the mitochondrial respiratory chain, whereas rotenone was used to inhibit complex I and to prevent accumulation of the SDH inhibitor oxaloacetate (39), enabling us to directly measure maximal SDH-driven respiration. We observed a dose depen-
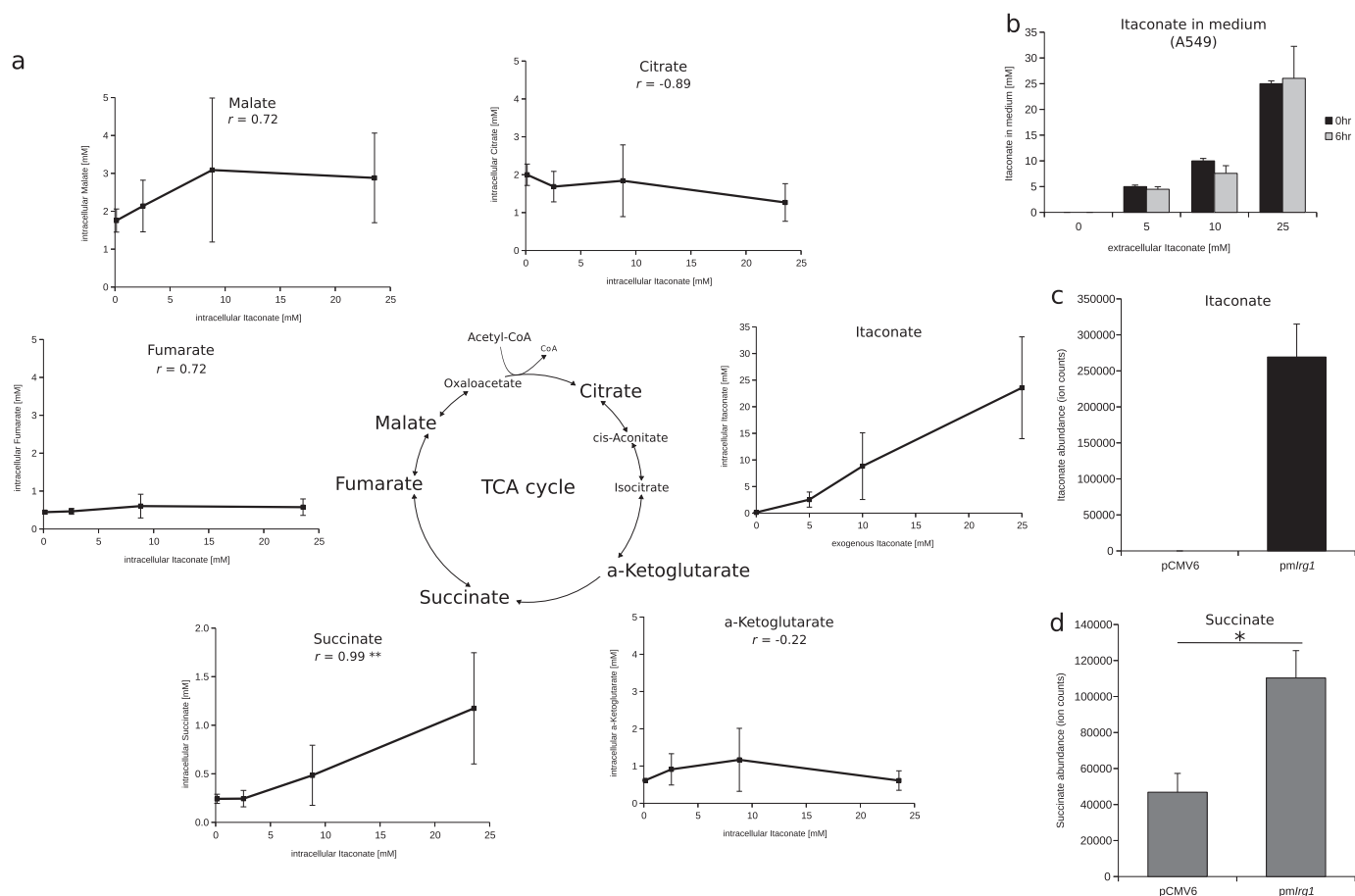
FIGURE 3. **Itaconate- and *Irg1*-induced succinate accumulation is not specific to immune cells.** *a*, intracellular itaconate and succinate levels increase in A549 lung adenocarcinoma cells after exposure to increasing exogenous itaconate concentrations (0, 5, 10, and 25 mM). Data represent the mean ± S.E. of metabolite levels [mM] of two repeated experiments with each three biological replicates. *b*, itaconate levels in medium after 6 h (*gray*) are not significantly affected compared with 0 h (*black*). Data represent the mean ± S.E. of metabolite levels of two repeated experiments with three biological replicates each. *c* and *d*, intracellular levels of itaconate (*c*, *black*) and succinate (*d*, *gray*) increased in *Irg1* overexpression A549 cells after transient transfection with murine pCMV6-*Irg1* overexpression (*pmIrg1*) plasmid compared with empty pCMV6-Entry (*pCMV6*) control plasmid. *Error bars* represent the intracellular metabolite levels (ion counts) 24 h after transfection of three biological replicates (mean ± S.E.). *, $p < 0.05$; **, $p < 0.01$.

dent inhibition of OCRs by itaconate in RAW 264.7 macrophages (Fig. 5*a*) and BMDMs (Fig. 5*b*), suggesting a regulatory role of itaconate for SDH activity. When the succinate concentration was lowered to 2.5 mM, itaconate had a greater proportional inhibitory effect. Considering the structural similarity of succinate to itaconate (also known as methylene succinate), our data suggest that itaconate acts as a competitive SDH inhibitor in immune cells, similar to the mechanisms described previously for the inhibition of purified SDH (27) and purified isocitrate lyase (22).

Next, to confirm that itaconate specifically inhibits SDH rather than other mitochondrial pathways, we offered permeabilized RAW 264.7 macrophages various oxidizable substrates and compared the maximal uncoupler-stimulated OCR in the presence of 0 and 10 mM itaconate (Fig. 5*c*). As expected, itaconate supplementation significantly reduced respiration (>75%) in the presence of succinate (SDH substrate) and rotenone (complex I inhibitor). On the other hand, oxygen consumption rates in permeabilized cells in the presence of either pyruvate with malate or glutamate with malate, substrates that drive respiration via complex I activity, were not affected by itaconate supplementation. Additionally, ascorbate and TMPD

were used to supply electrons for complex IV activity in the presence of antimycin A, an inhibitor of complex III. Itaconate also failed to impact this complex IV-mediated respiration. Together, these data provide evidence that itaconate contributes to succinate accumulation in macrophages by acting as an endogenous SDH inhibitor.

Loss of Irg1 Influences Succinate Levels in BMDMs—To determine how succinate levels are affected in the absence of endogenously produced itaconate, we analyzed BMDMs derived from *Irg1* KO mice. We confirmed that *Irg1* mRNA was not expressed in LPS-stimulated KO-derived BMDMs (Fig. 6*a*). Consistent with this result, LPS-stimulated BMDMs from *Irg1* KO mice failed to produce significant levels of itaconate (Fig. 6*b*). Notably, succinate concentrations in stimulated BMDMs from *Irg1* KO mice were significantly lower than those quantified in BMDMs from WT mice, suggesting that CAD-derived itaconate influences succinate accumulation in LPS-induced macrophages (Fig. 6*c*).

These results provide evidence that *Irg1*-mediated itaconate production plays a role in succinate accumulation within immune cells. Taken together, our data highlight a mechanistic function of itaconate whereby this metabolite acts as a SDH
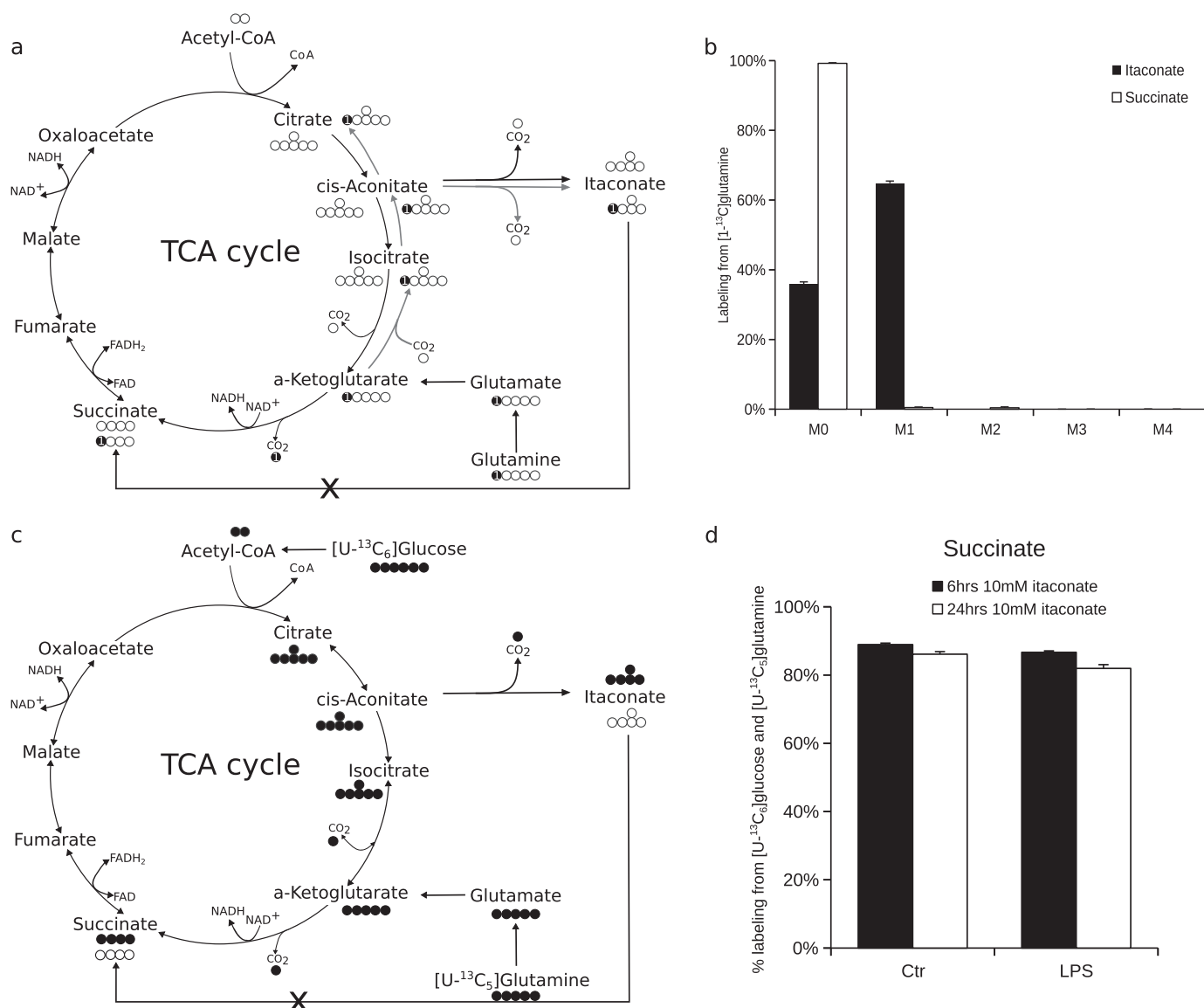
FIGURE 4. **Itaconate is not metabolized to succinate in RAW 264. 7 macrophages.** *a*, carbon labeling indicating oxidative (*black lines*) and reductive (*gray lines*) glutamine metabolism using [1-^{13}C]glutamine. Labeled itaconate (M1) is only synthesized through reductive glutamine metabolism (*gray*), and if it is metabolized to succinate, then it would result in succinate containing one labeled carbon (M1). *b*, mass isotopomer distribution of itaconate (*black*) and succinate (*white*) of LPS-activated RAW 264.7 macrophages after 24-h exposure to [1-^{13}C]glutamine tracer and 6-h exposure to 10 ng·ml^{-1} LPS. The major fraction of labeled itaconate contains one labeled carbon, whereas no labeling was found on succinate. *Error bars* represent the mean ± S.E. of mass isotopomer levels of three biological replicates. *c*, carbon labeling of TCA cycle intermediates using [U-^{13}C$_6$]glucose and [U-^{13}C$_5$]glutamine tracers. If exogenous, unlabeled itaconate is metabolized to succinate, then labeling would decrease but does not here. *d*, mass isotopomer distribution of succinate in resting and LPS-activated RAW 264.7 macrophages after 6-h (*black*) and 24-h (*gray*) exposure to exogenous, unlabeled itaconate remains ~90%, indicating that itaconate is not metabolized to succinate. Cells were prelabeled with [U-^{13}C$_6$]glucose and [U-^{13}C$_5$]glutamine over a period of three subcultures. *Error bars* represent the mean ± S.E. of mass isotopomer levels of three biological replicates.

inhibitor to influence TCA cycle metabolism by driving succinate accumulation (Fig. 7).

Discussion

Here we have demonstrated an important function of itaconate; it acts as a key regulatory metabolite to modulate TCA metabolism and succinate levels. In the cells studied, exogenous and endogenous, CAD-produced itaconate strongly correlated with succinate accumulation. Substrate-specific respirometry studies in permeabilized cells confirmed that itaconate acts as an SDH inhibitor. Finally, modulation of endogenous itaconate production in LPS-activated primary macrophages from *Irg1*

KO mice reduces succinate levels. Thus, itaconate alters mitochondrial metabolism to influence succinate accumulation in macrophages (Fig. 7).

Numerous metabolic pathways have been implicated in the metabolic reprogramming of immune cells, in particular those that regulate succinate levels, which, in turn, can influence HIF signaling or other pathways (13, 25, 40, 41). Glutamine serves as a major carbon source for succinate production in LPS-activated macrophages via α-ketoglutarate or, alternatively, through the GABA shunt (9). A recent systems-based analysis of macrophages under proinflammatory conditions described key break points in TCA metabolism at isocitrate dehydroge-
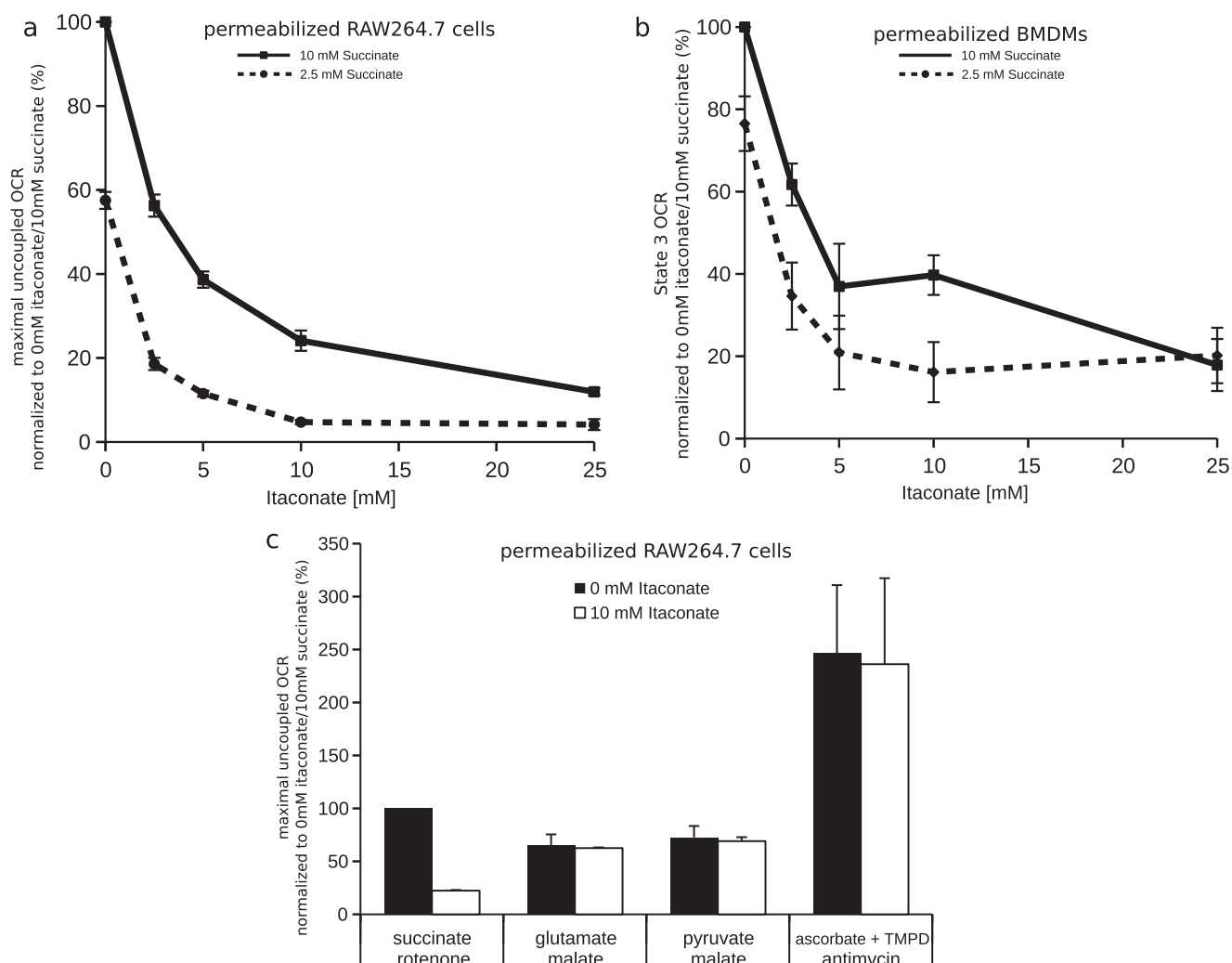
FIGURE 5. **Itaconate inhibits SDH.** *a* and *b*, itaconate inhibits the OCR in (*a*) RAW 264. 7 macrophages and (*b*) BMDMs in a dose-dependent manner. Shown are normalized OCRs of resting permeabilized cells exposed to increasing itaconate concentrations (0, 2.5, 5, 10, and 25 mM) with either 10 mM (*continuous line*) or 2.5 mM (*dashed line*) succinate. Data represent the mean $\pm$ S.E. of three repeated experiments. *c*, itaconate inhibits SDH of the respiratory chain. Shown is the normalized maximal uncoupled OCR of permeabilized resting RAW 264.7 macrophages exposed to various substrates in the presence of 0 mM (*black*) or 10 mM (*white*) itaconate. Data represent the mean $\pm$ S.E. of three repeated experiments normalized to conditions with 0 mM itaconate and 10 mM succinate.
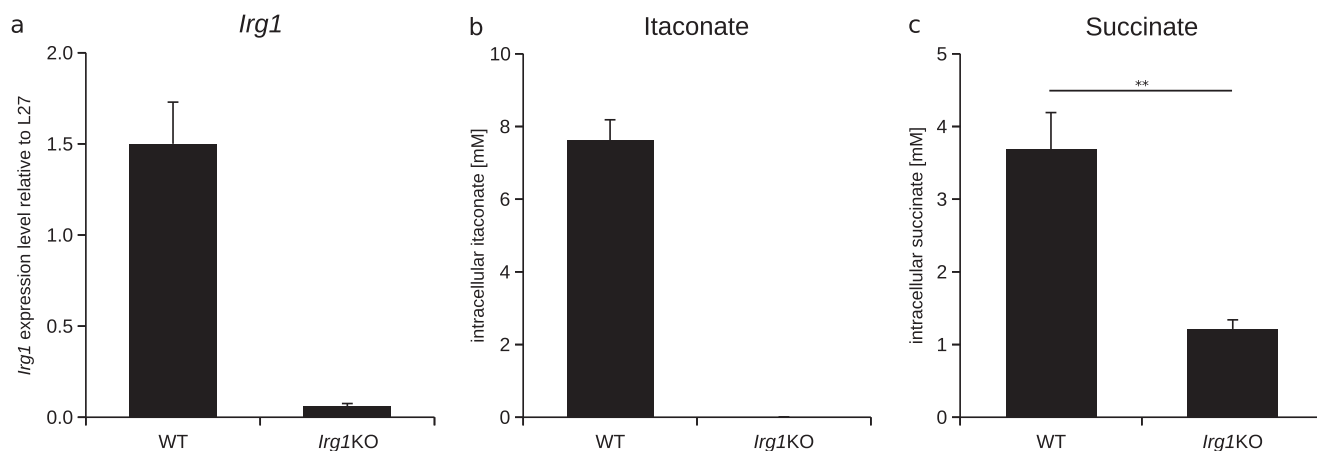

FIGURE 6. **Loss of *Irg1* decreases itaconate and succinate levels in *Irg1* KO BMDMs.** *a*, *Irg1* expression levels in LPS-activated (24 h, 10 ng·ml^{-1} LPS) BMDMs obtained from *Irg1* KO and WT mice. *Error bars* represent expression levels obtained from two independent mice (mean $\pm$ S.E.) relative to L27. *b* and *c*, itaconate and succinate levels in BMDMs obtained from *Irg1* KO and WT mice. Cells were activated for 6 h with 10 ng·ml^{-1} LPS. *Error bars* represent mean $\pm$ S.E. of metabolite levels [mM] of six biological replicates obtained from two independent mice.
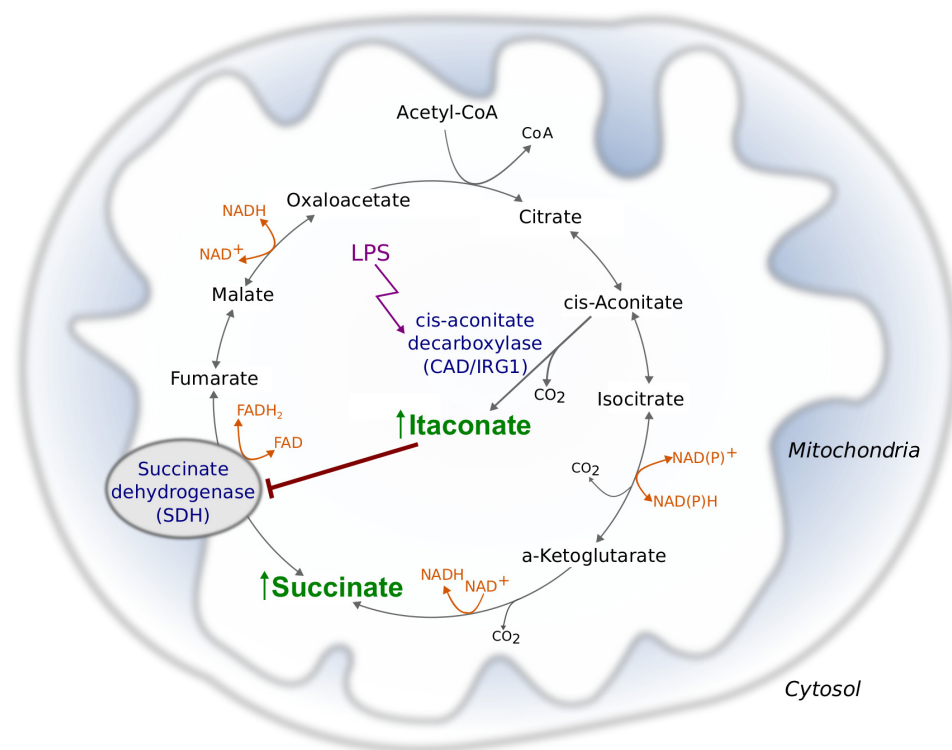
FIGURE 7. **Mechanism of LPS-induced succinate accumulation.** Under inflammatory conditions, such as LPS stimulation, mammalian CAD catalyzes the decarboxylation of the TCA cycle intermediate *cis*-aconitate to produce itaconate. This metabolite contributes to succinate accumulation in macrophages by acting as an endogenous SDH inhibitor.

nase and SDH (25). We have now identified a functional link between these nodes of the TCA cycle, where itaconate produced by mammalian CAD at the first break-point regulates SDH activity at the second break point. Within our analyses, we did observe variability in succinate accumulation upon LPS stimulation when comparing RAW 264.7 macrophages and BMDMs. This variance is in the range of succinate accumulation levels reported by others and is likely a function of cell, medium formulation, and LPS variability (9). However, we consistently observed increased succinate downstream of itaconate production or administration in a variety of cell types.

Succinate accumulation plays important roles during inflammation so that it contributes to the induction of *Il-1β* expression via HIF-1α stabilization (9). Our results suggest that *Irg1*-mediated itaconate production may influence downstream inflammatory responses in macrophages (*e.g.* expression of *Il-1β* or associated inflammatory genes). At present, it is not known whether this inflammatory response is accomplished directly by succinate or itaconate or mediated through other mechanisms. Succinate inhibits HIF-1α signaling through inhibition of PHD2 but can also impact the activity of numerous α-ketoglutarate-dependent dioxygenases (42, 43). As such, itaconate may have pleiotropic effects on cells depending on the expression, K_i, and compartment-specific impacts on succinate concentrations. However, the physiological role of itaconate and *Irg1* require further investigations, particularly in the context of macrophage development and differentiation. As noted above, various other pathways (*e.g.* GABA shunt, glutaminolysis) contribute to succinate synthesis in macrophages and could allow compensation (9, 13, 14). Intracellular signaling pathways

also play key roles in macrophage polarization and likely sustain inflammation to some degree in the absence of *Irg1* (44).

Given the diverse effects of inflammation in human disease, the mechanistic interplay between itaconate and succinate is of clinical interest. Itaconate was only recently identified as an endogenous mammalian biochemical (19), and subsequent studies demonstrated that this molecule was produced by mammalian CAD activity on *cis*-aconitate (20). Itaconate reprograms the metabolism of pathogens, such as *Mycobacterium tuberculosis*, by inhibition of isocitrate lyase, a key enzyme in the glyoxylate shunt (45); thus, macrophages produce the antimicrobial metabolite itaconate to combat against invading pathogens (20). Following these discoveries, it has recently been speculated that itaconate might contribute to the function of innate immune cells (2, 46). Importantly, *IRG1* is induced by various non-bacterial stimuli, including influenza A viral infection (47), Marek disease infection (48), during embryonic implantation (49), neurotropic viral infections of neurons (50), and in murine epidermal cells (51). Given the regulatory role of itaconate in succinate accumulation described here, *IRG1*-mediated itaconate production may act as a signaling molecule in other inflammatory situations or cellular states. Indeed, succinate can inhibit various other α-ketoglutarate-dependent dioxygenases to impact diverse cellular processes (42, 43). On the other hand, the mechanism outlined here for SDH inhibition could be used to mitigate pathogenic inflammation under certain circumstances (*e.g.* via CAD inhibition). For example, high levels of succinate have also been reported to occur under ischemic conditions because of reverse SDH activity (40, 41). The accumulated succinate is rapidly oxidized after reperfu-

sion, resulting in increased mitochondrial reactive oxygen species production and damage. A similar mechanism has been speculated to occur during sepsis (52). Notably, SDH inhibition protected against brain injury after ischemia/reperfusion (40, 41), suggesting that inhibition of SDH by endogenously produced itaconate may buffer against potential oxidative damage that can occur under such conditions.

Our findings provide critical new insights into the regulatory machinery governing TCA cycle function, with mammalian CAD-produced itaconate serving as a metabolic inhibitor to cause succinate accumulation. Ultimately, these results may be clinically important when drugs that target such metabolic inflammatory signals are identified. The emerging role of itaconate as a regulatory molecule to reprogram immune cell metabolism provides an intriguing link between innate immunity, metabolism, and disease pathogenesis.

References

1. Akira, S., Uematsu, S., and Takeuchi, O. (2006) Pathogen recognition and innate immunity. *Cell* **124,** 783–801

2. Kelly, B., and O'Neill, L. A. (2015) Metabolic reprogramming in macrophages and dendritic cells in innate immunity. *Cell Res.* **25,** 771–784

3. Krawczyk, C. M., Holowka, T., Sun, J., Blagih, J., Amiel, E., DeBerardinis, R. J., Cross, J. R., Jung, E., Thompson, C. B., Jones, R. G., and Pearce, E. J. (2010) Toll-like receptor-induced changes in glycolytic metabolism regulate dendritic cell activation. *Blood.* **115,** 4742–4749

4. Pearce, E. L., and Pearce, E. J. (2013) Metabolic pathways in immune cell activation and quiescence. *Immunity* **38,** 633–643

5. Rodríguez-Prados, J.-C., Través, P. G., Cuenca, J., Rico, D., Aragonés, J., Martín-Sanz, P., Cascante, M., and Boscá, L. (2010) Substrate fate in activated macrophages: a comparison between innate, classic, and alternative activation. *J. Immunol.* **185,** 605–614

6. Kempf, V. A., Lebiedziejewski, M., Alitalo, K., Wälzlein, J.-H., Ehehalt, U., Fiebig, J., Huber, S., Schütt, B., Sander, C. A., Müller, S., Grassl, G., Yazdi, A. S., Brehm, B., and Autenrieth, I. B. (2005) Activation of hypoxia-inducible factor-1 in bacillary angiomatosis: evidence for a role of hypoxia-inducible factor-1 in bacterial infections. *Circulation* **111,** 1054–1062

7. Blouin, C. C., Pagé, E. L., Soucy, G. M., and Richard, D. E. (2004) Hypoxic gene activation by lipopolysaccharide in macrophages: implication of hypoxia-inducible factor 1α. *Blood* **103,** 1124–1130

8. Hellwig-Bürgel, T., Rutkowski, K., Metzen, E., Fandrey, J., and Jelkmann, W. (1999) Interleukin-1β and tumor necrosis factor-α stimulate DNA binding of hypoxia-inducible factor-1. *Blood* **94,** 1561–1567

9. Tannahill, G. M., Curtis, A. M., Adamik, J., Palsson-McDermott, E. M., McGettrick, A. F., Goel, G., Frezza, C., Bernard, N. J., Kelly, B., Foley, N. H., Zheng, L., Gardet, A., Tong, Z., Jany, S. S., Corr, S. C., *et al.* (2013) Succinate is an inflammatory signal that induces IL-1β through HIF-1α. *Nature* **496,** 238–242

10. Selak, M. A., Armour, S. M., MacKenzie, E. D., Boulahbel, H., Watson, D. G., Mansfield, K. D., Pan, Y., Simon, M. C., Thompson, C. B., and Gottlieb, E. (2005) Succinate links TCA cycle dysfunction to oncogenesis by inhibiting HIF-alpha prolyl hydroxylase. *Cancer Cell* **7,** 77–85

11. Epstein, A. C., Gleadle, J. M., McNeill, L. A., Hewitson, K. S., O'Rourke, J.,

12. Mole, D. R., Mukherji, M., Metzen, E., Wilson, M. I., Dhanda, A., Tian, Y. M., Masson, N., Hamilton, D. L., Jaakkola, P., Barstead, R., Hodgkin, J., Maxwell, P. H., Pugh, C. W., Schofield, C. J., and Ratcliffe, P. J. (2001) C. elegans EGL-9 and mammalian homologs define a family of dioxygenases that regulate HIF by prolyl hydroxylation. *Cell* **107,** 43–54

13. Losman, J.-A., and Kaelin, W. G., Jr. (2013) What a difference a hydroxyl makes: mutant IDH, (R)-2-hydroxyglutarate, and cancer. *Genes Dev.* **27,** 836–852

14. Mills, E., and O'Neill, L. A. (2014) Succinate: a metabolic signal in inflammation. *Trends Cell Biol.* **24,** 313–320

15. Palsson-McDermott, E. M., Curtis, A. M., Goel, G., Lauterbach, M. A., Sheedy, F. J., Gleeson, L. E., van den Bosch, M. W., Quinn, S. R., Domingo-Fernandez, R., Johnson, D. G., Jiang, J. K., Israelsen, W. J., Keane, J., Thomas, C., Clish, C., *et al.* (2015) Pyruvate kinase M2 regulates Hif-1α activity and IL-1β induction and is a critical determinant of the Warburg effect in LPS-activated macrophages. *Cell Metab.* **21,** 65–80

16. Wegner, A., Meiser, J., Weindl, D., and Hiller, K. (2015) How metabolites modulate metabolic flux. *Curr. Opin. Biotechnol.* **34,** 16–22

17. Bailey, E., Stirpe, F., and Taylor, C. B. (1968) Regulation of rat liver pyruvate kinase. The effect of preincubation, pH, copper ions, fructose 1,6-diphosphate and dietary changes on enzyme activity. *Biochem. J.* **108,** 427–436

18. Chaneton, B., Hillmann, P., Zheng, L., Martin, A. C., Maddocks, O. D., Chokkathukalam, A., Coyle, J. E., Jankevics, A., Holding, F. P., Vousden, K. H., Frezza, C., O'Reilly, M., and Gottlieb, E. (2012) Serine is a natural ligand and allosteric activator of pyruvate kinase M2. *Nature* **491,** 458–462

19. Chaneton, B., and Gottlieb, E. (2012) Rocking cell metabolism: revised functions of the key glycolytic regulator PKM2 in cancer. *Trends Biochem. Sci.* **37,** 309–316

20. Strelko, C. L., Lu, W., Dufort, F. J., Seyfried, T. N., Chiles, T. C., Rabinowitz, J. D., and Roberts, M. F. (2011) Itaconic acid is a mammalian metabolite induced during macrophage activation. *J. Am. Chem. Soc.* **133,** 16386–16389

21. Michelucci, A., Cordes, T., Ghelfi, J., Pailot, A., Reiling, N., Goldmann, O., Binz, T., Wegner, A., Tallam, A., Rausell, A., Buttini, M., Linster, C. L., Medina, E., Balling, R., and Hiller, K. (2013) Immune-responsive gene 1 protein links metabolism to immunity by catalyzing itaconic acid production. *Proc. Natl. Acad. Sci. U.S.A.* **110,** 7820–7825

22. Patel, T. R., and McFadden, B. A. (1978) *Caenorhabditis elegans* and *Ascaris suum*: inhibition of isocitrate lyase by itaconate. *Exp. Parasitol.* **44,** 262–268

23. Williams, J. O., Roche, T. E., and McFadden, B. A. (1971) Mechanism of action of isocitrate lyase from *Pseudomonas indigofera*. *Biochemistry* **10,** 1384–1390

24. McFadden, B. A., and Purohit, S. (1977) Itaconate, an isocitrate lyase-directed inhibitor in *Pseudomonas indigofera*. *J. Bacteriol.* **131,** 136–144

25. O'Neill, L. A. (2015) A broken Krebs cycle in macrophages. *Immunity* **42,** 393–394

26. Jha, A. K., Huang, S. C., Sergushichev, A., Lampropoulou, V., Ivanova, Y., Loginicheva, E., Chmielewski, K., Stewart, K. M., Ashall, J., Everts, B., Pearce, E. J., Driggers, E. M., and Artyomov, M. N. (2015) Network integration of parallel metabolic and transcriptional data reveals metabolic modules that regulate macrophage polarization. *Immunity* **42,** 419–430

27. Booth, A. N., Taylor, J., Wilson, R. H., and Deeds, F. (1952) The inhibitory effects of itaconic acid *in vitro* and *in vivo*. *J. Biol. Chem.* **195,** 697–702

28. Ackermann, W. W., and Potter, V. R. (1949) Enzyme inhibition in relation to chemotherapy. *Proc. Soc. Exp. Biol. Med.* **72,** 1–9

29. Dervartanian, D. V., and Veeger, C. (1964) Studies on succinate dehydrogenase: I: spectral properties of the purified enzyme and formation of enzyme-competitive inhibitor complexes. *Biochim. Biophys. Acta.* **92,** 233–247

30. Raschke, W. C., Baird, S., Ralph, P., and Nakoinz, I. (1978) Functional macrophage cell lines transformed by Abelson leukemia virus. *Cell* **15,** 261–267

31. Giard, D. J., Aaronson, S. A., Todaro, G. J., Arnstein, P., Kersey, J. H., Dosik, H., and Parks, W. P. (1973) *In vitro* cultivation of human tumors: estab-

lishment of cell lines derived from a series of solid tumors. *J. Natl. Cancer Inst.* **51,** 1417–1423

31. Zhang, X., Goncalves, R., and Mosser, D. M. (2008) The isolation and characterization of murine macrophages. *Curr. Protoc. Immunol.* Chapter 14, Unit 14.1

32. Divakaruni, A. S., Rogers, G. W., and Murphy, A. N. (2014) Measuring mitochondrial function in permeabilized cells using the Seahorse XF analyzer or a Clark-type oxygen electrode. *Curr. Protoc. Toxicol.* **60,** 25.2.1–25.2.16

33. R Core Team (2013). *R: A language and environment for statistical computing,* R Foundation for Statistical Computing, Vienna, Austria

34. Cooper, R. A., and Kornberg, H. L. (1964) The utilization of itaconate by *Pseudomonas* sp. *Biochem. J.* **91,** 82–91

35. Adler, J., Wang, S.-F., and Lardy, H. A. (1957) The metabolism of itaconic acid by liver mitochondria. *J. Biol. Chem.* **229,** 865–879

36. Metallo, C. M., Gameiro, P. A., Bell, E. L., Mattaini, K. R., Yang, J., Hiller, K., Jewell, C. M., Johnson, Z. R., Irvine, D. J., Guarente, L., Kelleher, J. K., Vander Heiden, M. G., Iliopoulos, O., and Stephanopoulos, G. (2012) Reductive glutamine metabolism by IDH1 mediates lipogenesis under hypoxia. *Nature* **481,** 380–384

37. Németh, B., Doczi, J., Csete, D., Kacso, G., Ravasz, D., Adams, D., Kiss, G., Nagy, A. M., Horvath, G., Tretter, L., Mócsai, A., Csépányi-Kömi, R., Iordanov, I., Adam-Vizi, V., and Chinopoulos, C. (2015) Abolition of mitochondrial substrate-level phosphorylation by itaconic acid produced by LPS-induced Irg1 expression in cells of murine macrophage lineage. *FASEB J.* 10.1096/fj.15–279398

38. Degrandi, D., Hoffmann, R., Beuter-Gunia, C., and Pfeffer, K. (2009) The proinflammatory cytokine-induced IRG1 protein associates with mitochondria. *J. Interferon Cytokine Res.* **29,** 55–67

39. Wojtczak, L., Wojtczak, A. B., and Ernster, L. (1969) The inhibition of succinate dehydrogenase by oxaloacetate. *Biochim. Biophys. Acta* **191,** 10–21

40. Chouchani, E. T., Pell, V. R., James, A. M., Work, L. M., Saeb-Parsy, K., Frezza, C., Krieg, T., and Murphy, M. P. (2016) A unifying mechanism for mitochondrial superoxide production during ischemia-reperfusion injury. *Cell Metab.* **23,** 254–263

41. Chouchani, E. T., Pell, V. R., Gaude, E., Aksentijević, D., Sundier, S. Y., Robb, E. L., Logan, A., Nadtochiy, S. M., Ord, E. N. J., Smith, A. C., Eyassu, F., Shirley, R., Hu, C.-H., Dare, A. J., James, A. M., *et al.* (2014) Ischaemic accumulation of succinate controls reperfusion injury through mitochondrial ROS. *Nature* **515,** 431–435

42. Xiao, M., Yang, H., Xu, W., Ma, S., Lin, H., Zhu, H., Liu, L., Liu, Y., Yang, C., Xu, Y., Zhao, S., Ye, D., Xiong, Y., and Guan, K.-L. (2012) Inhibition of α-KG-dependent histone and DNA demethylases by fumarate and succinate that are accumulated in mutations of FH and SDH tumor suppressors. *Genes Dev.* **26,** 1326–1338

43. Metallo, C. M., and Vander Heiden, M. G. (2013) Understanding metabolic regulation and its influence on cell physiology. *Mol. Cell* **49,** 388–398

44. Sica, A., and Mantovani, A. (2012) Macrophage plasticity and polarization: *in vivo veritas. J. Clin. Invest.* **122,** 787–795

45. Eoh, H., and Rhee, K. Y. (2014) Methylcitrate cycle defines the bactericidal essentiality of isocitrate lyase for survival of *Mycobacterium tuberculosis* on fatty acids. *Proc. Natl. Acad. Sci. U.S.A.* **111,** 4976–4981

46. Cordes, T., Michelucci, A., and Hiller, K. (2015) Itaconic acid: the surprising role of an industrial compound as a mammalian antimicrobial metabolite. *Annu. Rev. Nutr.* **35,** 451–473

47. Preusse, M., Tantawy, M. A., Klawonn, F., Schughart, K., and Pessler, F. (2013) Infection- and procedure-dependent effects on pulmonary gene expression in the early phase of influenza A virus infection in mice. *BMC Microbiol.* **13,** 293

48. Smith, J., Sadeyen, J.-R., Paton, I. R., Hocking, P. M., Salmon, N., Fife, M., Nair, V., Burt, D. W., and Kaiser, P. (2011) Systems analysis of immune responses in Marek's disease virus-infected chickens identifies a gene involved in susceptibility and highlights a possible novel pathogenicity mechanism. *J. Virol.* **85,** 11146–11158

49. Cheon, Y.-P., Xu, X., Bagchi, M. K., and Bagchi, I. C. (2003) Immune-responsive gene 1 is a novel target of progesterone receptor and plays a critical role during implantation in the mouse. *Endocrinology.* **144,** 5623–5630

50. Cho, H., Proll, S. C., Szretter, K. J., Katze, M. G., Gale, M., Jr., and Diamond, M. S. (2013) Differential innate immune response programs in neuronal subtypes determine susceptibility to infection in the brain by positive-stranded RNA viruses. *Nat. Med.* **19,** 458–464

51. Hall, C. J., Boyle, R. H., Sun, X., Wicker, S. M., Misa, J. P., Krissansen, G. W., Print, C. G., Crosier, K. E., and Crosier, P. S. (2014) Epidermal cells help coordinate leukocyte migration during inflammation through fatty acid-fuelled matrix metalloproteinase production. *Nat. Commun.* **5,** 3880

52. Bar-Or, D., Carrick, M. M., Mains, C. W., Rael, L. T., Slone, D., and Brody, E. N. (2015) Sepsis, oxidative stress, and hypoxia: are there clues to better treatment? *Redox Rep.* **20,** 193–197